

# First results on light readout from the 1-ton ArDM liquid argon detector for dark matter searches

**C. Amsler<sup>a</sup>, A. Badertscher<sup>b</sup>, V. Boccone<sup>a</sup>, A. Bueno<sup>c</sup>, M. C. Carmona-Benitez<sup>c</sup>, W. Creus<sup>a</sup>, A. Curioni<sup>b</sup>, M. Daniel<sup>d</sup>, E. J. Dawe<sup>e</sup>, U. Degunda<sup>b</sup>, A. Gendotti<sup>b</sup>, L. Epprecht<sup>b</sup>, S. Horikawa<sup>b</sup>, L. Kaufmann<sup>b</sup>, L. Knecht<sup>b</sup>, M. Laffranchi<sup>b</sup>, C. Lazzaro<sup>b</sup>, P. K. Lightfoot<sup>e</sup>, D. Lussi<sup>b</sup>, J. Lozano<sup>c</sup>, A. Marchionni<sup>b</sup>, K. Mavrokoridis<sup>e</sup>, A. Melgarejo<sup>c</sup>, P. Mijakowski<sup>f</sup>, G. Natterer<sup>b</sup>, S. Navas-Concha<sup>c</sup>, P. Otyugova<sup>a</sup>, M. de Prado<sup>d</sup>, P. Przewlocki<sup>f</sup>, C. Regenfus<sup>a</sup>, F. Resnati<sup>b</sup>, M. Robinson<sup>e</sup>, J. Rochet<sup>a</sup>, L. Romero<sup>d</sup>, E. Rondio<sup>f</sup>, A. Rubbia<sup>b</sup>, L. Scotto-Lavina<sup>a</sup>, N. J. C. Spooner<sup>e</sup>, T. Strauss<sup>b</sup>, J. Ulbricht<sup>b</sup>, and T. Viant<sup>b</sup> (The ArDM Collaboration)**

<sup>a</sup>Physik-Institut, University of Zürich, Winterthurerstrasse 190, CH-8057 Zürich, Switzerland

<sup>b</sup>ETH Zurich, Institute for Particle Physics, CH-8093 Zürich, Switzerland

<sup>c</sup>University of Granada, Dpto. de Física Teórica y del Cosmos & C.A.F.P.E, Campus Fuente Nueva, 18071 Granada, Spain

<sup>d</sup>CIEMAT, Div. de Física de Partículas, Avda. Complutense, 22, E-28040, Madrid, Spain

<sup>e</sup>University of Sheffield, Department of Physics and Astronomy, Hicks Building, Hounsfield Road, Sheffield, S3 7RH, UK

<sup>f</sup>The Andrzej Soltan Institute for Nuclear Studies, Hoża 69, 00-681 Warsaw, Poland

**ABSTRACT:** ArDM-1t is the prototype for a next generation WIMP detector measuring both the scintillation light and the ionization charge from nuclear recoils in a 1-ton liquid argon target. The goal is to reach a minimum recoil energy of 30 keVr to detect recoiling nuclei. In this paper we describe the experimental concept and present results on the light detection system, tested for the first time in ArDM on the surface at CERN. With a preliminary and incomplete set of PMTs, the light yield at zero electric field is found to be between 0.3-0.5 phe/keVee depending on the position within the detector volume, confirming our expectations based on smaller detector setups.

**KEYWORDS:** Photon detectors for VUV, UV, photomultipliers, scintillators, noble liquids, liquid argon, wavelength shifters, WIMP detectors, dark matter.

---

## Contents

<b>1. Introduction</b>	<b>1</b>
<b>2. Detector</b>	<b>2</b>
<b>3. Performance of the light readout system</b>	<b>4</b>
3.1 Monte Carlo simulation	8
3.2 Completion of the light readout with 14 PMTs	10
<b>4. Conclusions</b>	<b>10</b>

---

## 1. Introduction

Astronomical observations give strong evidence for the existence of non-luminous and non-baryonic Dark Matter, presumably composed of a new type of elementary particle. It is of utmost importance to experimentally verify if Dark Matter is indeed composed of the leading candidate called the Weakly Interacting Massive Particle (WIMP) [1]. If such WIMPs exist and are sufficiently stable, they would form a cold thermal relic gas in the present universe. Direct detection is achieved by observing the energy deposited when they scatter elastically from target nuclei, and with a cross-section magnitude which is predicted to be weak-like. This requires the capability of measuring a few events with recoil energies in the region of a few tens of keV and with negligible backgrounds from other natural sources of radiation. Assuming a “canonical” WIMP halo model and a mass of 100 GeV, a WIMP-proton cross-section of  $10^{-44} \text{ cm}^2 = 10^{-8} \text{ pb}$  would yield about 1 recoil event per day per ton of argon above 30 keVr. The direct laboratory detection of WIMPs is a necessary complement to e.g. SUSY searches actively pursued at the LHC.

The Argon Dark Matter 1-ton detector (ArDM-1t) is a liquid argon (LAr) double-phase time projection chamber for direct dark matter searches [2]. The goal is to design, assemble and operate a ton-scale liquid argon detector with independent ionization and scintillation readouts – complementary to other single and double phase noble liquid gas experiments like DEAP-CLEAN [3] and WARP [4] using argon, and XENON[5], XMASS [6] and ZEPLIN-III [7] using xenon – and to demonstrate the feasibility of an argon-based ton-scale experiment for WIMP detection, with good detection efficiency and high background discrimination. A 1-ton prototype is presently installed on the surface at CERN, and has been operated for the first time in single-phase light collection mode, while double-phase operation is in preparation.

Substantial R&D efforts were needed to develop the light readout of ArDM-1t, justifying the operation of the detector first on the surface, where many functionalities could more easily be tested, before moving to an underground location for physics runs in low background conditions. The developments that resulted in the definition of the ArDM reflector were reported in [8]. In this paper, we present results obtained during the first operation of the light detection system fully embedded in the ArDM-1t vessel.

## 2. Detector

Figure 1 shows a conceptual layout of the apparatus. The sensitive liquid argon volume diameter, delimited by the wavelength shifter reflectors, is 80 cm and the maximal drift length is 120 cm. The ultra-clean liquid argon in the detector is provided and maintained by a cryogenic and purification system separated from the main dewar to allow the insertion of a radiation shield against neutrons (See Figure 2). Charged particles lead to ionization and excitation of argon atoms, forming eximers. The luminescence is detected by an array of photomultipliers immersed in the liquid at the bottom of the detector, while the charge (electron cloud) is drifted in a strong electric field towards a charge amplifying readout system located in the vapor phase above the liquid argon.

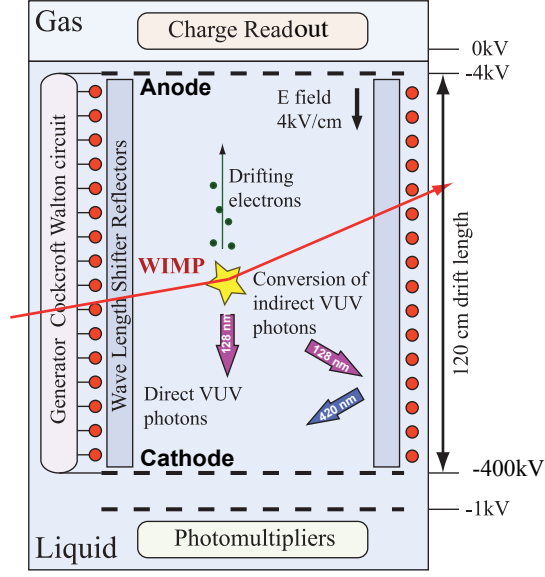


**Figure 1.** Conceptual layout of the ArDM experiment.

The basic mechanisms by which slow ionizing particles lead to ionization and scintillation signals in liquid argon in energy regions of tens of keV are not well known. However, to define the needed performance of the detector, it is sufficient to assume that a WIMP-induced nuclear recoil of 30 keVr will produce around 300 VUV photons (at 128 nm), together with a few free ionization electrons, the latter number depending on the electric field strength due to electron-ion recombination [9]. For background discrimination (e.g. from background  $\gamma$ 's), 30 keVr recoils should be compared to an electronic energy deposition of  $30 \text{ keVr} \times L_{eff} \approx 7.5 \text{ keVee}^1$ , which will generate several hundreds of free ionization electrons. In addition, a fast (few ns) and a slow ( $\sim 1.6 \mu\text{s}$ ) component of the scintillation light are observed in liquid argon [11], their ratio also depending on the ionizing type. Therefore, the charge/light ratio [12, 13] and pulse shape discrimination [14, 15] provide efficient discrimination against gamma or beta electron recoils. Heavily ionizing particles such as  $\alpha$ 's or nuclear recoils contribute mostly to the fast decaying component, while the contribution of electrons and  $\gamma$ 's to the slow component is larger. Quantitatively, the component ratio

<sup>1</sup>The ratio of the nuclear recoil scintillation response to the electronic recoil response was recently measured to be  $0.25 \pm 0.02 \pm 0.01$  (correlated) for recoils above 20 keVr. See Ref. [10].

$CR$  of the fast ( $< 50$  ns) to the total intensity is typically 0.8 for heavily and 0.3 for minimum ionizing projectiles. Measurements at low energy show mean values within 0.6-0.7(nuclear recoils) and 0.36-0.28(electronic recoils) in the energy range 7-32 keVee [15]. The higher ratio of light to charge production for nuclear recoils, and the corresponding higher component ratio, can both be used to reduce background in WIMP searches.

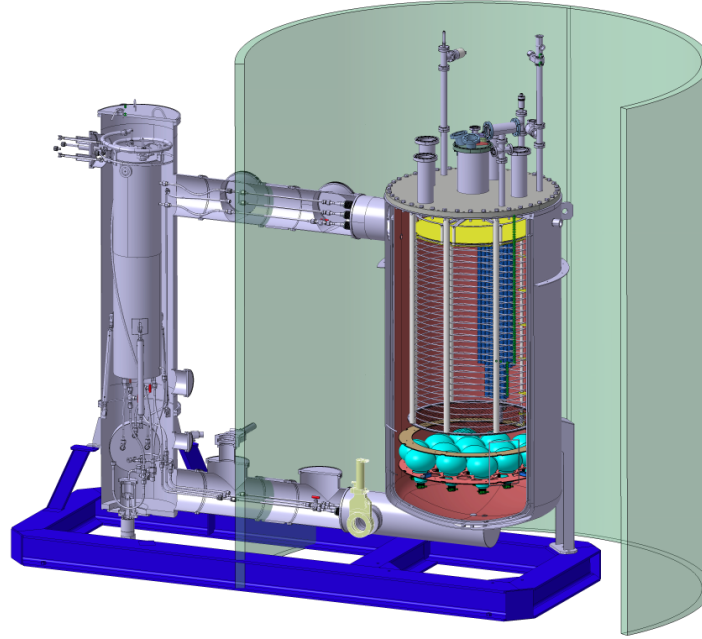


**Figure 2.** 3D model of the cryo-system, main dewar and detector components. The main vessel inner diameter is 100 cm and the maximal drift length is 120 cm. Yellow: charge readout system, cyan : light readout PMTs, green : outer dimension of neutron shield.

A Greinacher (Cockroft-Walton) generator chain, as described in Ref. [16], is immersed in the liquid and is able to provide a field up to about 3 kV/cm to avoid electron-ion recombination and to drift the electrons to the top surface of the liquid towards the gas phase. At the interface, the electrons are extracted to the gas phase and accelerated towards the Large Electron Multiplier (LEM [17–19] or THGEM [20–22]), which provides multiplication and position reconstruction by a segmented anode. A 3D image of the event is thus obtained with a much lower energy threshold than in a single phase liquid argon time projection chamber, allowing for example to detect multiple nuclear recoils as expected from fast neutrons entering the detector. This information will be used to estimate the irreducible single recoil neutron background by direct extrapolation from the observed multiple scatter events, which constitute more than 50% of the neutron induced events within the large active volume of ArDM-1t [23].

The 128 nm VUV light is emitted isotropically from the interaction point and converted to blue (420 nm) light by a wavelength shifter (WLS) deposited on reflectors mounted on the side walls which also define the fiducial volume [8]. The reflectors consist of Tetratex (TTX) foils,  $254 \mu\text{m}$  thick, which have nearly 100% diffuse Lambertian reflectance. A surface density of  $1 \text{ mg/cm}^2$  of

TetraPhenyl Butadiene (TPB) was evaporated on these foils [24]. In the completed detector, the shifted and reflected light is collected at the bottom of the cryostat by 14 photomultiplier tubes (PMT, 8" Hamamatsu R5912-02MOD with bialkali photocathodes and Pt-underlay) immersed in the liquid. Each PMT is soldered with its leads onto a 3 mm thick printed circuit board, providing also the individual mechanical footing and the voltages for cathode and dynodes with passive electronic components. A support structure holding up the fourteen 8" PMTs was built to sustain the total buoyant force in LAr ( $\approx 60$  kg) under the constraint of minimal amount of material. It was manufactured out of a 5 mm thick stainless steel disk by cutting out hexagonal holes. The individual PMT units were fixed to this plate by 3 screws through their PCB bases on the bottom.

A WLS deposition on the PMT glass ( $0.05 \text{ mg/cm}^2$  of TPB) was also performed to improve the direct VUV light detection. To optimize the light readout, a range of reflectors and WLS depositing combinations were investigated with several small prototypes, in which argon scintillation light was generated by radioactive sources in gas at normal temperature and pressure [25]. A detailed comparison is reported in Refs. [8] and [26].

### 3. Performance of the light readout system

After a several-month-long ultra-high vacuum evacuation of the main detector vessel, which removed outgassing from detector surfaces and materials, certified leak-tightness and finally resulted in a residual pressure  $\ll 10^{-5}$  mbar in the full volume encompassing the detector and the purification circuit, a four weeks engineering run of ArDM-1t with a preliminary version of the light readout took place for the first time in spring 2009. This first run was preceded by a careful assessment of the cryogenic requirements and the related safety issues.

Large amounts of calibration data with different radioactive sources were collected. During this first run a reduced temporary set of 7 PMTs with various surface treatments (sand-blasted or transparent glass, no PMT surface coating, TPB-Paraloid coating or TPB-evaporation – for details on the various methods see Ref. [8]) was installed to test the efficiency for the direct light detection (an 8th PMT was installed but could not be operated due to HV problems) [27]. The used PMT array and support structure are shown in fig. 3, and specification details are given in Table 1. These measurements indicated a slightly better performance (at the 10 % level) from evaporating a thin layer of TPB on the PMT entrance windows instead of coating them with a thin TPB-Paraloid layer. The first process could also be done with better uniformity. More details on this as well as comparative measurements in gaseous argon can be found in [26]. Figure 3 (right) shows the lateral WLS foils under UV illumination before insertion into the cryostat.

Each PMT was individually fed from one HV channel of a CAEN SY2527 system and read out by a 10 bit FADC channel (1Gs/s) from an ACQIRIS DC 282 system. The system could be triggered internally e.g. by requiring at least 2 PMTs with a signal over threshold, or externally, e.g. tagging an external radioactive source (see below).

The gain of the PMTs was determined from the average single photon charge observed from short light pulses generated by an internally mounted LED (400 nm) placed in the vapor region above the liquid argon surface. Figure 4 (left) shows the measured gain  $G$  as a function of applied high voltage for the 7 temporary PMTs immersed in LAr for several days. The data points were fitted with the function  $G = A \cdot V^{kn}$ , where  $n$  is the number of dynodes and  $A, k$  are fit parameters.

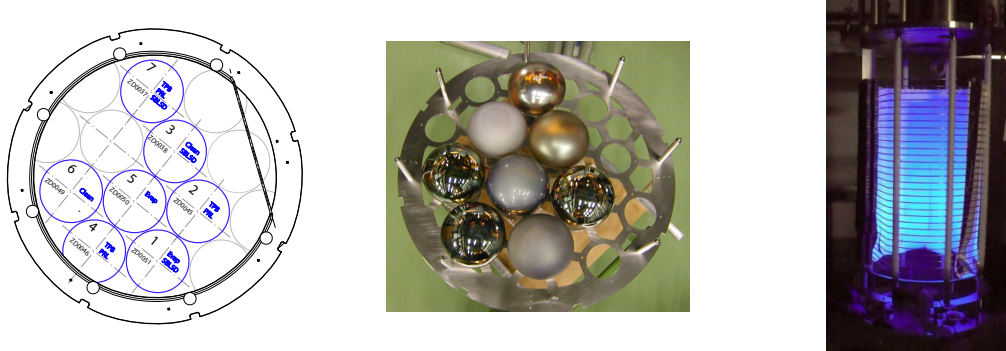


**Figure 3.** Left: schematic showing position of the temporary 7 PMTs as listed in Table 1. Middle: photograph showing the top view of the temporary 7 PMT array used for the first measurements in liquid argon. Right: photograph showing the TPB covered lateral TTX foils within the drift field shaper ring electrodes, illuminated with UV light.

#	type	dynodes	window	coating	max. gain
1	Hamamatsu R5912-02MOD	14	Sandblasted	TPB evaporated	$\approx 1 \cdot 10^9$
2	Hamamatsu R5912-02MOD	14	Transparent	TPB-Paraloid	$\approx 1 \cdot 10^9$
3	Hamamatsu R5912-MOD	10	Sandblasted	No coating	$\approx 5 \cdot 10^7$
4	Hamamatsu R5912-02MOD	14	Transparent	TPB-Paraloid	$\approx 1 \cdot 10^9$
5	Hamamatsu R5912-02MOD	14	Transparent	TPB evaporated	$\approx 1 \cdot 10^9$
6	Hamamatsu R5912-02MOD	14	Transparent	No coating	$\approx 1 \cdot 10^9$
7	Hamamatsu R5912-MOD	10	Sandblasted	TPB-Paraloid	$\approx 5 \cdot 10^7$

**Table 1.** Properties of the cryogenic hemispherical 8'' PMTs installed in the LAr detector.

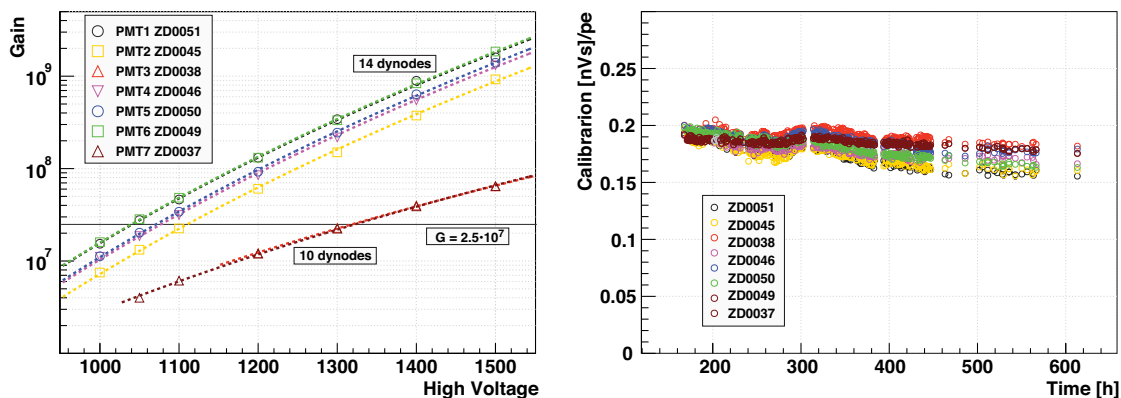


**Figure 4.** Left: Gain curves of the PMTs in LAr. The curves are fits to the data points (see text). Right: Time evolution of the calibration of the PMTs during the run in nVs/photoelectron (p.e.).

At the beginning of the run the PMT gains were set to  $2.5 \cdot 10^7$  by adjusting individually the bias voltages. This value corresponds to an average integrated signal of 0.2 nVs per photoelectron and was matching our desired dynamic range. The number of photoelectrons collected by each PMT was determined from the integrated charge measured over a  $50 \, \Omega$  resistor. Figure 4 (right) shows the time evolution of the calibration constants during the full duration of the run. The small drift



is attributed to slow temperature and pressure fluctuations introducing mechanical stress on the dynode chain of the PMT, and appears to level off after some time in stable working conditions. It can be accounted for during the offline analysis.

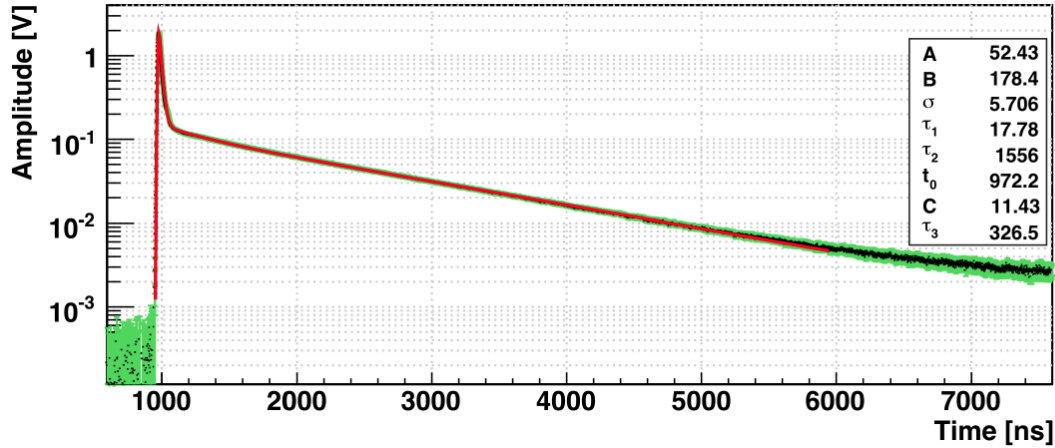


**Figure 5.** Time distribution in LAr. The red curve is a fit with three exponential decay functions.

Figure 5 shows a typical time distribution of the signal in the detector for electrons,  $\gamma$ 's and cosmic muons which were selected by the component ratio  $CR < 0.4$ . The data were taken with the internal trigger by setting the discriminator thresholds to 50 mV. A fit with three exponential decay functions leads to an excellent description of the observed average waveform data, with measured lifetimes  $\tau_1 = 17.8 \pm 1.0$  ns for the fast component,  $\tau_2 = 1556 \pm 10$  ns for the slow component, and  $\tau_3 = 326 \pm 10$  ns for the intermediate one, with contributions of 21, 74 and 5%, respectively [26].

No attempt was made to deconvolute the response of the PMTs and the acquisition system in  $\tau_1$ , while the fitted  $\tau_2$  was used to qualify the achieved purity of the liquid argon in our setup, a very relevant quantity for the performance of light and charge collection. Indeed, the mean lifetime  $\tau_2$  of the slow scintillation component is very sensitive to traces of impurities and can be used to monitor the LAr purity. This effect was studied in gaseous argon (see ref. [28] for details) and similar observations are made in liquid [26, 29]. Accordingly, the LAr purity was studied and monitored over several weeks by measuring  $\tau_2$  with radioactive sources. A single exponential fit to the average pulse distribution at later times was applied since  $\tau_2$  does not depend on the type of ionizing particle. Figure 6 shows the time dependence of  $\tau_2$  during the run (600h). Our average-over-time result (fit dashed line)  $\tau_2 = 1.540 \pm 0.009$   $\mu$ s is in good agreement with expectations and consistent with no significant deterioration of purity over several weeks of operation. From the observed lifetime of the slow component, we estimate that the concentration of  $N_2$  and  $O_2$  was consistent with being less than 0.1 ppm [26, 29] Hence the detector was satisfactorily tight and clean, although the active LAr recirculation system was not yet operated.

We now present our first evaluation of the detector performance with respect to light yield and detection efficiency of low energy events, which were the two main goals pursued during this first engineering run. The measurements were performed with external radioactive sources at zero electric field. For the measurements presented here a 20 kBq  $^{22}\text{Na}$   $\gamma$ -source was employed,

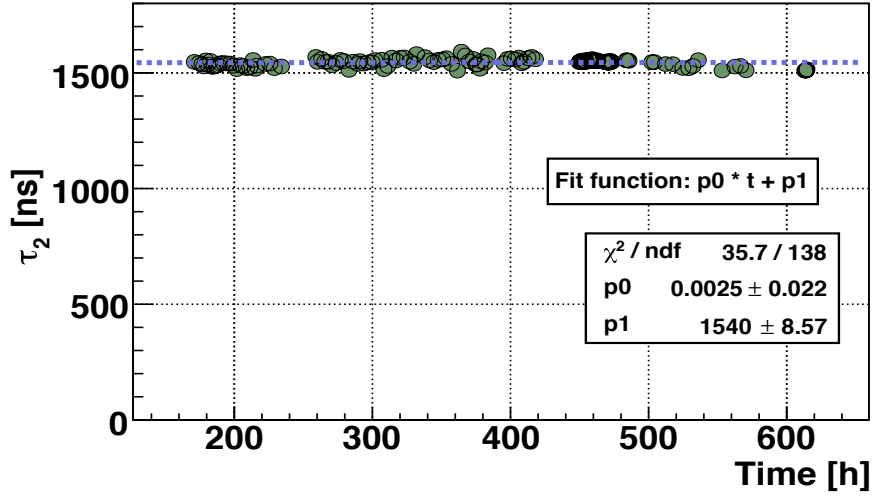


**Figure 6.** Evolution of the lifetime  $\tau_2$  of the slow scintillation component during the run. The dashed line is a straight line fit revealing good purity conditions.

delivering positrons (annihilating into two 511 keV  $\gamma$ 's) and monochromatic 1275 keV  $\gamma$ 's. The light yield produced by one of the 511 keV  $\gamma$ 's, following (multiple) Compton scattering, was measured by triggering with a 4" NaI(Tl) scintillation crystal on the second 511 keV emitted in the opposite direction, and on the 1275 keV  $\gamma$ . A sketch of the experimental arrangement is shown in fig. 7.

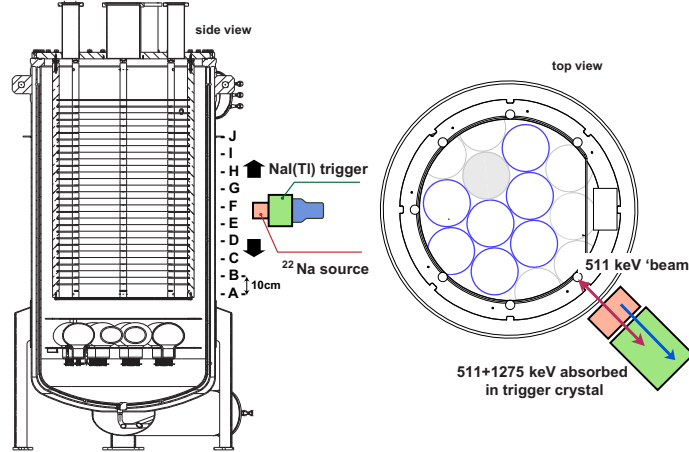


**Figure 7.** Sketch of the apparatus used to measure the light yield in liquid argon with an external  $^{22}\text{Na}$   $\gamma$ -source and a triggering NaI(Tl) crystal.

The PMT array at the bottom of the apparatus is meant to measure the scintillation light with good time resolution. Single photon counting is possible with a signal-to-noise ratio of around 20,



the limiting noise being generated at the input stage of the FADCs. The coincidence of at least 2 PMT signals within typically 10 – 1000 ns was used as the event trigger and initiated the readout of 10000 FADC samples, corresponding to a 10  $\mu$ s long interval at 1 Gs/s with 1000 (9000) samples before (after) the trigger time.

Rather than summing the digitized samples to recover the PMT measured light intensity, which due to the slow component of argon has a long tail of decaying amplitude, the time digitized waveforms were analysed offline to identify “charge clusters” coming from groups of photons or from single photons. The individual charge clusters were then added in an optimized time window of 4500 ns located around the peak found with maximum amplitude, to obtain integrated pulse heights. This method is very efficient in the case of the long decay time of argon, and was found to yield an integration error coming from electronic noise and accidental dark counts of about 1.4 p.e. (rms) at high energies, reaching the limit of 1/20 p.e. for single photons. These values were determined from random empty events collected 10  $\mu$ s before the signal trigger. The pedestal of each PMT was determined on an event-by-event basis in an iterative way from the time distributions in the first 600 ns before trigger time.

### 3.1 Monte Carlo simulation

A full Monte Carlo (MC) simulation of the ArDM detector has been developed [23, 30]. The code, based on GEANT4 [31], includes tracking of all particles through a detailed detector geometry description and has in addition a full simulation of the light propagation and detection in ArDM (isotropic emission of the primary scintillation light, VUV propagation, wavelength shifting, surface optical properties, reflections, and PMT response). The following assumptions were made:

- The absorption of VUV or optical photons in LAr is neglected; Rayleigh scattering is included [32];
- The wavelength shifting efficiency of the side reflectors and of the PMTs coating (TPB) was 100%;
- The diffuse reflection coefficient of the side reflectors was varied between 88% and 98%, with a value of 95% giving the best description of the experimental data;
- The maximum quantum efficiencies of the PMTs were between 18.5% and 22%, according to the data sheets of each PMT, and the quantum efficiency over the photocathode surfaces were parameterized as a function of the polar angle, with a maximum on the vertical ( $\theta = 0$ ), decreasing by about 30% for large  $\theta$ ;

These assumptions are in good agreement with our own measurements on smaller prototypes in the laboratory [8, 33]. For instance, our measurements were 95% for the diffuse reflection coefficient and typically 15% for the quantum efficiency integrated over  $\theta$ . In addition, outside the GEANT4 MC:

- A Gaussian noise smearing of 1.4 p.e. was applied to MC data;
- The measured values were corrected to compensate for our chosen finite integration time of 4500 ns.

These MC predictions, expressed in numbers of photoelectrons could then be compared directly with data. For the absolute direct comparison with the external sources, the MC simulation was extended to include the test setup shown in fig. 7, including the acceptance of the NaI(Tl) trigger counter. The  $^{22}\text{Na}$  external source was taken into account by simulating a 511 keV  $\gamma$  emitted in a cone covering the NaI solid angle. Data taken with the  $^{22}\text{Na}$ -source at different heights were directly compared with MC simulated data and could be absolutely normalized, since the detection efficiency of the 511 keV photon inside ArDM-1t was accordingly properly included in the MC. The same selection cuts were applied to the data and MC.

Figure 8 shows the light yield distributions for the four positions (see fig. 7) B, D, F and G (black bars), absolutely normalized to the MC. The light yield (in p.e.) was also calculated by MC simulation (95% reflectivity) as a function of energy deposit, and the distributions (red line) compared to the measured ones. Good agreement is found, with discrepancies of less than 10% in the light yield. The drops in the spectra around 200 – 300 p.e. correspond to full absorption of the 511 keV photon in the fiducial volume. No clear full energy peak is visible due to the fact the most of the 511 keV photons undergo multiple interactions and are not fully absorbed. The width of the peak at zero photoelectrons is determined from events collected with a special trigger setup, acquiring events happening 10  $\mu\text{s}$  before the actual trigger, i.e. empty events, to take into account dark counts and accidental pileup.

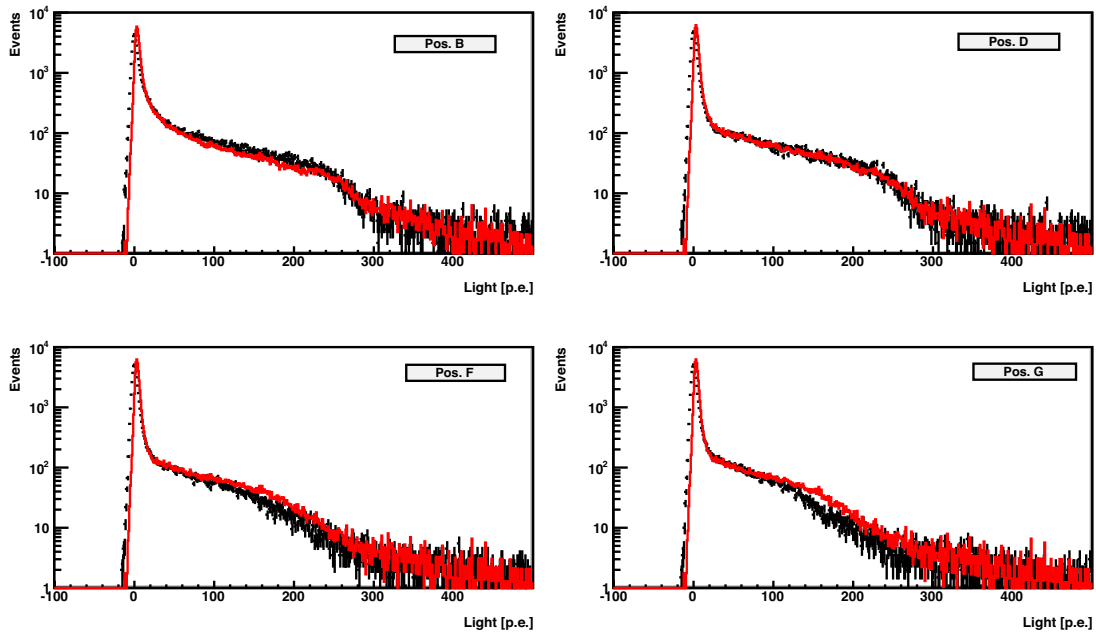


**Figure 8.** Light detection in the ArDM-1t detector for 511 keV  $\gamma$ 's, in photoelectrons at the positions B, D, F, G of the  $^{22}\text{Na}$ - source (see fig. 7). The measurements are shown in black with error bars, the simulated data in red. The data were triggered by the coincident absorption of a 511 and a 1275 keV  $\gamma$  in the external trigger NaI(Tl) crystal.

A general trend of the spectra at the various source positions is the lower light yield for events occurring in the upper part of the detector, which is well described by the MC simulation (however, we expect this effect to be less pronounced in the completed detector which will include the charge

readout, due to downward reflection of the wavelength shifted light from the reflective charge readout surface).

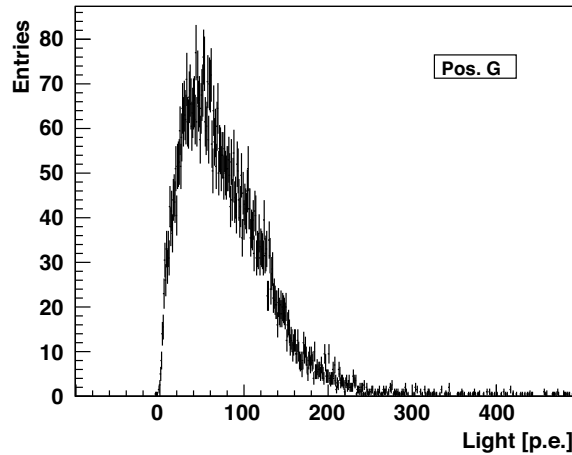


**Figure 9.** Pulse area (p.e.) distribution of electron recoil events close to the reconstruction threshold.

Since our MC simulation reproduces well our data, we can estimate the absolute light yield per unit energy for electron recoils from it. We find that the average light yield varies between 0.3-0.5 p.e./keVee with the temporary 7 PMTs configuration. This is roughly half of the yield that would be obtained with a completed detector with 14 PMTs. Since the light yield for nuclear recoils is lower due to quenching, and is typically 25% that for electrons in the few 10 keV range [10], we expect from these first measurements to detect 30 keVr nuclear recoils with an average signal of 6 photoelectrons and a resolution of about 40%.

For completeness, the energy distribution for events passing the trigger conditions of at least two coincident photoelectrons within 10 ns is plotted in fig. 9. This also shows that reconstructing events down to a few keV is feasible. Further work will be performed to improve the trigger at low energy (this was not achievable during our first test on surface due to the very high count rate from ambient backgrounds) once the detector is underground, in a low background environmental condition.

### 3.2 Completion of the light readout with 14 PMTs

The light detection system with 14 PMTs was completed recently. Figure 10 (left) shows the arrangement under illumination with a UV hand held light source, to demonstrate the wavelength shifting behavior of the coatings. Figure 10 (right) displays the results from a test in gaseous argon with a vertically movable 5.3 MeV Am  $\alpha$ -source. The light distributions are as expected, showing the homogeneous response of the 14 PMTs when the source is not too close to their surfaces.

## 4. Conclusions

Summarizing, we have for the first time experimentally demonstrated that the detection of low energy depositions as those expected from nuclear recoils is feasible in the ArDM-1t detector, and

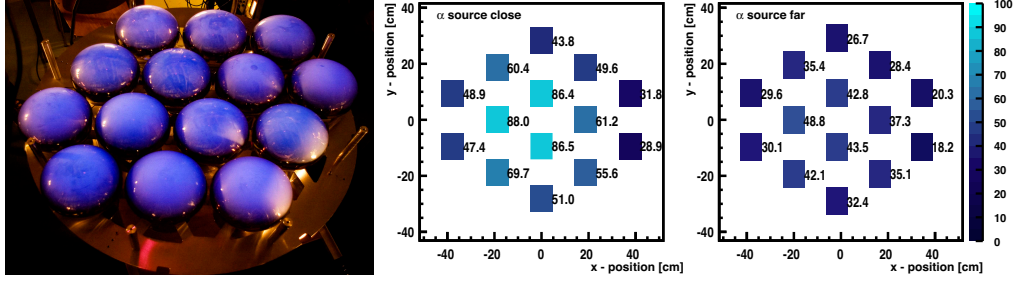


**Figure 10.** Array of 14 cryogenic PMTs under UV illumination. The two plots on the right show the detected light intensity (in p.e.) on the PMTs from the near and far  $\alpha$ -source in gaseous argon.

we have measured the time and amplitudes distribution of argon luminescence during a month long calibration run. The long term purity of the cryogenic system has been established from the continuous monitoring of the slow component of the LAr scintillation light. With half of the foreseen light collection system installed, a light yield averaged over the active volume of 0.4 photoelectron/keV for electron recoils (at zero electric field) has been measured. Most important, we have reached a good understanding of the light propagation and detection in our detector, fully implemented in a detailed Monte Carlo simulation.

## Acknowledgments

This work was supported by ETH Zürich, the University of Zürich and the Swiss National Science Foundation (SNF). We are grateful to CERN for their hospitality where the tests on surface could be performed, and thank the thin film and surface workshop of A. Braem at CERN for the coating of the PMTs windows.

## References

- [1] G. Steigman and N.S. Turner, *Cosmological constraints on the properties of weakly interacting massive particles*, Nucl. Phys. B **B253** (1985) 375.
- [2] A. Rubbia, *ArDM: A ton-scale liquid argon experiment for direct detection of dark matter in the universe*, J. Phys. Conf. Ser. **39** (2006) 129 [hep-ph/0510320].
- [3] M. Boulay *et al.* [ DEAP-CLEAN Collaboration ], *Dark matter search at SNOLAB with DEAP-1 and DEAP/CLEAN-3600*, J. Phys. Conf. Ser. **136**, 042081 (2008).
- [4] P. Benetti *et al.*, *Astropart. Phys.* **28** (2007) 495.
- [5] E. Aprile [ Xenon Collaboration ], *The XENON100 dark matter experiment at LNGS: Status and sensitivity*, J. Phys. Conf. Ser. **203**, 012005 (2010).
- [6] Y. Suzuki [ XMASS Collaboration ], *XMASS experiment*, PoS **IDM2008**, 001 (2008).
- [7] D. Y. Akimov *et al.*, *The ZEPLIN-III dark matter detector: instrument design, manufacture and commissioning*, *Astropart. Phys.* **27**, 46-60 (2007). [astro-ph/0605500].
- [8] V. Boccone *et al.*, *Development of wavelength shifter coated reflectors for the ArDM argon dark matter detector*, JINST **4** (2009) P06001.

- [9] R. Chandrasekharan, *Design of the Light Readout for the ArDM Experiment*, PhD thesis, Diss. ETH No. 16985 (2007).
- [10] D. Gastler, E. Kearns, A. Hime *et al.*, *Measurement of scintillation efficiency for nuclear recoils in liquid argon* [arXiv:1004.0373 [physics.ins-det]].
- [11] A. Hitachi *et al.*, *Effect of ionization density on the time dependence of luminescence from liquid argon and xenon*, Phys. Rev. **27** (1983) 5279.
- [12] A. S. Barabash, A. I. Bolozdynya, *How To Detect The Dark Matter Of The Galaxy If It Is Made Up Of Weakly Interacting Neutral Particles With Masses  $1\text{-GeV}/c^2$  -  $10\text{-GeV}/c^2$* , JETP Lett. **49**, 356-359 (1989).
- [13] A. Benetti *et al.*, *Detection of energy deposition down to the keV region using liquid xenon scintillation*, Nucl. Instrum. Meth. A **327** (1993) 203.
- [14] M. G. Boulay and A. Hime, *Technique for direct detection of weakly interacting massive particles using scintillation time discrimination in liquid argon*, Astropart. Phys. **25**, 179 (2006).
- [15] W. H. Lippincott, K. J. Coakley, D. Gastler *et al.*, *Scintillation time dependence and pulse shape discrimination in liquid argon*, Phys. Rev. **C78**, 035801 (2008). [arXiv:0801.1531 [nucl-ex]].
- [16] S. Horikawa *et al.*, *Feasibility of high-voltage systems for a very long drift in liquid argon TPCs*, to appear in Proc. of 1st International Workshop towards the Giant Liquid Argon Charge Imaging Experiment (GLA2010), Tsukuba (Japan), March 2010 [arXiv:1009.4908 [physics.ins-det]].
- [17] P. Otyugova, *Development of a Large Electron Multiplier (LEM) based charge readout system for the ArDM experiment*, PhD thesis, Diss. ETH No. 17704, 2008.
- [18] A. Badertscher *et al.*, *Operation of a double-phase pure argon Large Electron Multiplier Time Projection Chamber: comparison of single and double phase operation*, Nucl. Instrum. Meth. A **617**, 188 (2010) [arXiv:0907.2944 [physics.ins-det]].
- [19] A. Badertscher *et al.*, *Construction and operation of a Double Phase LAr Large Electron Multiplier Time Projection Chamber*, To appear in the proceedings of 2008 IEEE Nuclear Science Symposium (NSS) and Medical Imaging Conference (MIC) and 16th International Workshop on Room-Temperature Semiconductor X-Ray and Gamma-Ray Detectors (RTSD), Dresden, Germany, 18-25 Oct 2008. arXiv:0811.3384 [physics.ins-det].
- [20] A. Breskin *et al.*, *A concise review on THGEM detectors*, Nucl. Instrum. Meth. A **598** (2009) 107 [arXiv:0807.2026 [physics.ins-det]].
- [21] R. Alon *et al.*, *Operation of a thick gas electron multiplier (THGEM) in Ar, Xe and Ar-Xe*, JINST **3** (2008) P01005.
- [22] A. Bondar, A. Buzulutskov, A. Grebenuk, D. Pavlyuchenko, Y. Tikhonov and A. Breskin, *Thick GEM versus thin GEM in two-phase argon avalanche detectors*, JINST **3** (2008) P07001 [arXiv:0805.2018 [physics.ins-det]].
- [23] L. Kaufmann, *Detector Performance and Background Studies for the ArDM Experiment*, PhD thesis, ETH Zurich, 2008.
- [24] H. Cabrera, *Optimierung des Wellenlängenschiebers für das ArDM-Experiment*, Master Thesis, University of Zürich, 2007.
- [25] A. Büchler, *The beginning of a dark matter adventure*, Bachelor Thesis, University of Zürich, 2006; M. Thomann, *Wave Length Shifting Reflectors in Liquid Argon for the ArDM Experiment*, Bachelor Thesis, University of Zürich, 2008.

- [26] V. Boccone, *Development of the Light Readout for the ArDM Dark Matter Search*, PhD Thesis, University of Zürich, 2010.
- [27] F. Resnati *et al.* [ArDM Collaboration], *The ArDM Experiment* to appear in Proc. of 8th international workshop on Identification of Dark Matter (IDM2010), Montpellier, France; U. Degunda, in *ArDM: Double Phase Argon Calorimeter and TPC for Direct Detection of DM at TeV Particle Astrophysics* 2010, Paris, France; M. Haranczyk *et al.* [ArDM Collaboration], *The ArDM experiment*, Acta Phys. Polon. B **41**, 1441 (2010) [arXiv:1006.5335 [physics.ins-det]]; C. Amsler, *ArDM, a 1t liquid argon detector for dark matter searches*, Proc. of Science PoS (EPS-HEP 2009)110; V. Boccone, *Test in Liquid Argon of the Light Readout System for the ArDM Experiment*, IEEE Nucl. Science Symp. Conf. Rec., Orlando N25-153 (2009); P. Otyugova, *The ArDM - a ton - scale liquid argon experiment for direct Dark Matter Detection*, 5th Patras Workshop on Axions, WIMPs and WISPs (2009); C. Regenfus, *The Argon Dark Matter Experiment*, Proc. of TAUP2009, arXiv:0912.2962v1 [phys.ins-det] 2009
- [28] C. Amsler *et al.*, *Luminescence quenching of the triplet excimer state by air traces in gaseous argon*, JINST **3** (2008) P02001.
- [29] R. Acciarri *et al.*, *Effects of nitrogen and oxygen contaminations in liquid argon*, Nucl. Instrum. Meth. **A607** (2009) 169.
- [30] M. del Carmen Carmona-Benitez, *Direct Dark Matter Searches with Noble Liquid Detectors: The ArDM Experiment*, PhD thesis, Universidad de Granada, 2009.
- [31] S. Agostinelli *et al.*, *GEANT4 - a simulation toolkit*, Nucl. Instrum. Meth. **A506** (2003) 250.
- [32] G. M. Seidel, R. E. Lanou and W. Yao, *Rayleigh scattering in rare-gas liquids*, Nucl. Instrum. Meth. **A489** (2002) 189 [arXiv:hep-ex/0111054].
- [33] A. Bueno, J. Lozano, A. J. Melgarejo, F. J. Munoz, J. L. Navarro, S. Navas and A. G. Ruiz, *Characterization of large area photomultipliers and its application to dark matter search with noble liquid detectors*, JINST **3** (2008) P01006 [arXiv:0711.3592 [physics.ins-det]].